Neuron
Article

Translocation of a "Winner" Climbing Fiber to the Purkinje Cell Dendrite and Subsequent Elimination of "Losers" from the Soma in Developing Cerebellum

Kouichi Hashimoto,[1,2,3,6] Ryoichi Ichikawa,[4,6] Kazuo Kitamura,[1,2] Masahiko Watanabe,[5] and Masanobu Kano[1,2,*]
[1]Department of Neurophysiology, Graduate School of Medicine, The University of Tokyo, 7-3-1 Hongo, Tokyo 113-0033, Japan
[2]Department of Cellular Neuroscience, Graduate School of Medicine, Osaka University, 2-2 Yamada-oka, Suita 565-0871, Japan
[3]Core Research for Evolutional Science and Technology (CREST), Japan Science and Technology Agency, Tokyo 102-8666, Japan
[4]Department of Anatomy, Sapporo Medical University School of Medicine, Sapporo 060-8556, Japan
[5]Department of Anatomy, School of Medicine, Hokkaido University, Sapporo, 060-8638, Japan
[6]These authors contributed equally to this work
*Correspondence: mkano-tky@m.u-tokyo.ac.jp
DOI 10.1016/j.neuron.2009.06.008

SUMMARY

Functional neural circuits are formed by eliminating early-formed redundant synapses and strengthening necessary connections during development. In newborn mouse cerebellum, each Purkinje cell (PC) is innervated by multiple climbing fibers (CFs) with similar strengths. Subsequently, a single CF is selectively strengthened by postnatal day 7 (P7). We find that this competition among multiple CFs occurs on the soma before CFs form synapses along dendrites. Notably, in most PCs, the single CF that has been functionally strengthened (the "winner" CF) undergoes translocation to dendrites while keeping its synapses on the soma. Synapses of the weaker CFs (the "loser" CFs) remain around the soma and form "pericellular nests" with synapses of the winner CFs. Then most perisomatic synapses are eliminated nonselectively by P15. Thus, our results suggest that the selective translocation of the winner CF to dendrites in each PC determines the single CF that survives subsequent synapse elimination and persistently innervates the PC.

INTRODUCTION

Proper functions of the nervous system rely on the precise formation of neural circuits during development. At birth, neurons have redundant synaptic connections not only to their proper targets but also to other cells. Then, functional neural circuits are formed during early postnatal development by the selective strengthening and stabilization of necessary synapses, and the weakening and pruning of surplus connections (Hensch, 2004; Katz and Shatz, 1996; Lichtman and Colman, 2000; Purves and Lichtman, 1980). The climbing fiber (CF) to Purkinje cell (PC) synapse of the cerebellum has been a good system for the study of developmental refinement of neural circuits in the CNS (Crepel, 1982; Hashimoto and Kano, 2005; Hashimoto et al., 2009; Lohof et al., 1996). PCs are initially innervated by multiple CFs that originate from different neurons in the inferior olivary nuclei. Surplus CFs are gradually eliminated during early postnatal development and most PCs in mice become innervated by single CFs by the end of the third postnatal week (Kano et al., 1995, 1997, 1998; Offermanns et al., 1997).

Our previous study indicates that each PC is initially innervated by multiple CFs with similar synaptic strengths, and that a single CF is selectively strengthened relative to other CFs during the first postnatal week (Hashimoto and Kano, 2003). This "winner" CF can widely innervate the PC dendritic tree and is presumed to become the monoinnervating CF in the adult. Morphological evidence indicates that the site of CF innervation of PC undergoes a change from soma to dendrite, a phenomenon termed "CF translocation" (Altman, 1972; Altman and Bayer, 1997; Chedotal and Sotelo, 1992; Kiyohara et al., 2003; Larramendi, 1969; Mason et al., 1990; Palay and Chan-Palay, 1974; Ramón y Cajal, 1911; Sugihara, 2005). However, it remains unclear how the functional strengthening of a single CF is correlated with the morphological translocation of CF synapses from soma to dendrite. It is crucial to determine whether CF translocation results from the competition of multiple CFs on dendrites (i.e., more than one CF undergo translocation to dendrites), or only the winner CF extends its innervation to dendrites after "defeating" the other CFs at synaptic competition on the soma. It is also unclear how redundant CF synapses are eliminated after CF translocation.

In the present study, we used both electrophysiological and morphological techniques and examined when and how CF translocation occurs. We found that all CFs had their synaptic terminals around PC somata and formed pericellular nests at P7–P8 when a single CF had already been strengthened among multiple CFs innervating the same PC (Hashimoto and Kano, 2003). At P9, CFs that elicited the largest excitatory postsynaptic currents (EPSCs) started to extend their synapses along PC dendrites while keeping their somatic synapses until around P12. In contrast, synaptic terminals of the other CFs that elicited smaller EPSCs were confined to the soma and the basal part of the primary dendrite. Importantly, these weaker CFs were collaterals of the strongest CFs innervating adjacent PCs. Then, CF monoinnervation of PC was established around P15 by nonselective elimination of perisomatic synapses originating from

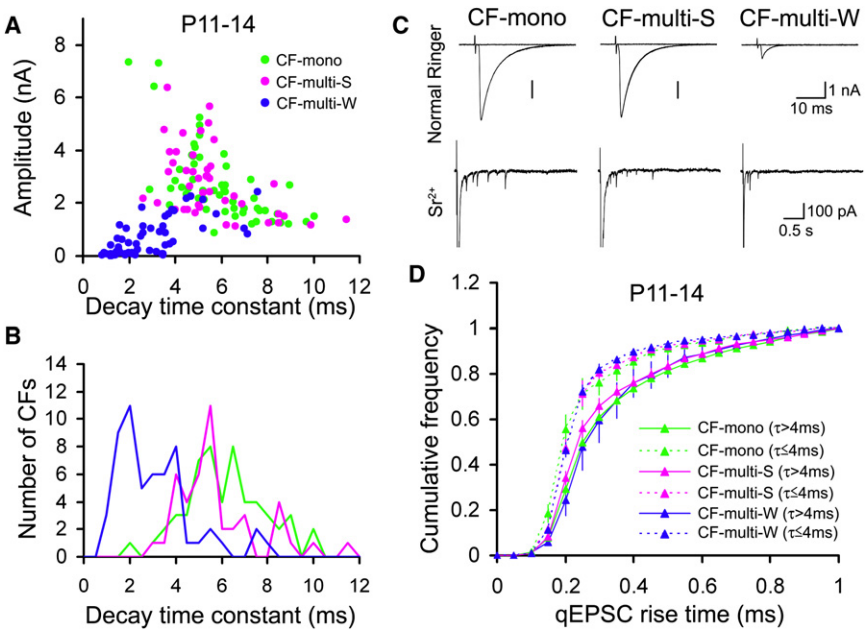

Figure 1. Classification of CFs Based on the Decay Time Constants of Evoked EPSCs and the 10%–90% Rise Times of qEPSCs Arising from the Stimulated CFs at P11–P14

(A) The CF-EPSC amplitude is plotted against the decay time constant. Data were sampled from lobule III–VI in the cerebellar vermis at P11–P14. Data for CF-mono, CF-multi-S, and CF-multi-W are shown as green, pink, and blue circles, respectively.

(B) Frequency distribution of CF inputs in terms of the decay time constants of EPSCs evoked by stimulating individual CFs. Data for CF-mono, CF-multi-S, and CF-multi-W are shown as green, pink, and blue lines, respectively.

(C) (Upper) Representative traces of EPSCs evoked by stimulating CF-mono, CF-multi-S, and CF-multi-W in normal Ringer solution. EPSCs for CF-multi-S and CF-multi-W were recorded from the same PC. Two to three traces are superimposed at each threshold stimulus intensity. CFs were stimulated in the granule cell layer at 0.2 Hz. Holding potential was –20 mV. For this and following figures, the holding potential was corrected for liquid-junction potential. (Lower) Asynchronous qEPSCs elicited in the Sr^{2+}-containing solution. Holding potential was −90 mV.

(D) Average cumulative histograms for the 10%–90% rise times of qEPSCs arising from CF-mono ($\tau > 4$ ms) (green solid line, n = 24), CF-multi-S ($\tau > 4$ ms) (pink solid line, n = 19), CF-multi-W ($\tau > 4$ ms) (blue solid line, n = 4), CF-mono ($\tau \leq 4$ ms) (green broken line, n = 3), CF-multi-S ($\tau \leq 4$ ms) (pink broken line, n = 3), and CF-multi-W ($\tau \leq 4$ ms) (blue broken line, n = 14) at P11–P14. Values are expressed as mean ± SEM.

both the strongest and weaker CFs. Thus, CF synapse refinement in each PC is considered to proceed in the following order: (1) competition among CFs on the soma, (2) translocation of the single winner CF to the dendrite, and (3) elimination of the "loser" CFs from the soma.

RESULTS

Waveforms of CF-EPSCs Reflect CF Synapse Locations on the Somato-Dendritic Domain of PCs

Since development of the cerebellum proceeds from ventral to dorsal lobules (Altman and Bayer, 1997; Sugihara, 2005), we confined the area of electrophysiological and morphological analyses to lobule III–VI to avoid possible interlobular differences. After P7, each PC is either monoinnervated by a strong CF (CF-mono) or multiply innervated by a strong CF (CF-multi-S) and a few weaker CFs (CF-multi-W) (Hashimoto et al., 2001; Hashimoto and Kano, 2003). As an indicator of maturation of synaptic function, we measured kinetics of EPSCs elicited by stimulating these three types of CFs and examined differences among them. Waveforms of CF-mediated EPSCs (CF-EPSCs) are affected by the location of CF synapses on PC dendrites because of the filtering caused by space-clamp error (Hashimoto et al., 2001; Roth and Hausser, 2001). In the somatic voltage-clamp configuration, synaptic responses elicited at distal dendrites suffer from stronger distortions than those at proximal dendrites. As a result of such distortions, the peak amplitude is attenuated, the rising phase is slowed, and the decay time is prolonged (Hashimoto et al., 2001; Roth and Hausser, 2001). Thus, locations of CF synapses on PCs can be estimated electrophysiologicaly from the rise time and the decay time constant of CF-EPSCs (Hashimoto et al., 2001; Roth and Hausser, 2001).

We first investigated CF innervation patterns of PCs at P11–14 after the initiation of CF translocation to PC dendrites (Chedotal and Sotelo, 1992; Mason et al., 1990). At this stage, most CF-EPSCs (99.9%) had a 10%–90% rise time shorter than 1 ms, regardless of their peak amplitudes (Table S1 available online) (Hashimoto et al., 2001; Hashimoto and Kano, 2003). Since CF-EPSCs generated at distal dendrites have rise times longer than 1 ms under voltage-clamp recordings from the soma (Hashimoto et al., 2001; Miyazaki et al., 2006), the present result suggests that all CFs form their synapses on the soma and proximal dendrites of PCs at P11–P14. In the following experiments, only CF-EPSCs with a rise time shorter than 1 ms were analyzed.

Predominant CFs Have Expanded Their Innervation Territories to PC Dendrites at P11–P14

We plotted the peak amplitudes of CF-EPSCs against their decay time constants (Figure 1A). Distributions of the data points for CF-mono and CF-multi-S were almost overlapped, indicating that kinetic profiles of EPSCs for CF-mono and CF-multi-S were similar (Figures 1A and 1B). In contrast, EPSCs for CF-multi-W had smaller amplitudes and faster decays when compared to those for CF-mono and CF-multi-S (Figures 1A and 1B). There is a clear distinction between the distribution of decay time constants of evoked EPSCs for CF-mono or CF-multi-S and that for CF-multi-W at around 4 ms (Figures 1A and 1B). Despite some overlap, the majority of EPSCs for CF-mono (87.3%, n = 55) and CF-multi-S (81.4%, n = 43) had decay time constants longer than 4 ms, whereas the majority of EPSCs for CF-multi-W

(85.7%, n = 56) had decay time constants shorter than 4 ms. Furthermore, as shown below (Figure S4 available online), our analysis of the correlation between the decay time constant of CF-EPSCs and the total CF length along PC dendrites indicates that decay time constants for CFs that form terminals beneath the basal part of the primary dendrites are estimated to be shorter than 4.8 ms. Therefore, the decay time constant of around 4 ms appears to be the dividing point between the CFs that are presumed to extend their synapses to dendrites and the CFs whose synapses appear to be confined to PC somata. Therefore, in the rest of the present study at P11–P14, we divided each of the three CF groups (CF-mono, CF-multi-S, and CF-multi-W) into two subgroups at the decay time constant of 4 ms.

Although the decay time constants of EPSCs evoked by CF stimulation reflect locations of synapses along the somatodendritic domain of PCs, this parameter is also affected by factors other than dendritic filtering, such as asynchronous release of synaptic vesicles and altered clearance of transmitters (Edmonds et al., 1995; Wadiche and Jahr, 2001). At adult CF synapses, multiple synaptic vesicles are fused simultaneously to the presynaptic terminal membrane and release glutamate, a phenomenon known as multivesicular release (Hashimoto and Kano, 2003; Wadiche and Jahr, 2001). High glutamate concentration transients resulting from multivesicular release may prolong decay times of EPSCs (Wadiche and Jahr, 2001). Therefore, to estimate locations of CF synapses from CF-EPSC waveforms, it is necessary to analyze the kinetics of EPSCs arising from single synaptic vesicles in CF terminals. In a Sr^{2+}-containing external solution, stimulation of a CF elicits quantal EPSCs (qEPSCs) arising from the stimulated CF because of enhanced asynchronous release of synaptic vesicles (Hashimoto and Kano, 2003). We analyzed waveforms of qEPSCs arising from individual CFs and estimated the extent of CF translocation using the following rationale. Under somatic voltage-clamp, qEPSCs originating from dendrites are strongly attenuated by dendritic filtering (Lisman et al., 2007), as suggested by previous experimental (Smith et al., 2003) and theoretical (Roth and Hausser, 2001) studies. Because CFs that have undergone translocation to PC dendrites have synapses with different electrotonic lengths from the somatic recording site, individual qEPSCs should undergo different degrees of distortion depending on the locations of CF synapses on PC dendrites. In contrast, CFs confined to perisomatic regions have synapses with short electrotonic lengths from the recording site, and distortions of qEPSC waveforms for such somatic CFs should be minimal. Thus, we can estimate the locations of CF synapses along the somatodendritic domain of PCs by analyzing distortions of qEPSC kinetics. We used the 10%–90% rise time of qEPSCs rather than the decay time constant because the rise time is reported to be more proportional to the distance from the synaptic sites to the soma when compared to the decay time constant (Roth and Hausser, 2001).

Based on this rationale, we examined CF innervation patterns at P11–P14. In a subset of PCs, individual CFs were separately stimulated in the Sr^{2+}-containing external solution and qEPSCs arising from the stimulated CFs were recorded (Figure 1C, see Experimental Procedures). Consistent with our previous report, amplitudes of qEPSCs for CF-mono and CF-multi-S tended to be slightly smaller than those for CF-multi-Ws, although there was no significant difference in statistics (Hashimoto and Kano, 2003) (data not shown). Figure 1D shows cumulative plots of the 10%–90% qEPSC rise time for the six types of CFs. Rise times for the CFs with decay time constants of evoked CF-EPSCs longer than 4 ms (CF-mono [$\tau > 4$ ms], CF-multi-S [$\tau > 4$ ms], and CF-multi-W [$\tau > 4$ ms]) showed similar distributions with relatively high incidences of qEPSCs with slow rise times (Figure 1D). In contrast, qEPSCs with slow rise times were much less frequent for the CFs with decay time constants shorter than 4 ms (CF-mono [$\tau \leq 4$ ms], CF-multi-S [$\tau \leq 4$ ms], and CF-multi-W [$\tau \leq 4$ ms]) in comparison to the CFs with decay time constants longer than 4 ms (Figure 1D). To quantify the extent of CF translocation to PC dendrites, we averaged the 10%–90% rise times of qEPSCs arising from each CF (Table S2). The average qEPSC rise times for CF-multi-S ($\tau > 4$ ms) and CF-multi-W ($\tau > 4$ ms) were not significantly different from the value for CF-mono ($\tau > 4$ ms) (Table S2). In contrast, the average qEPSC rise time was significantly shorter in CF-mono ($\tau \leq 4$ ms), CF-multi-S ($\tau \leq 4$ ms), and CF-multi-W ($\tau \leq 4$ ms) than in CF-mono ($\tau > 4$ ms) (Table S2).

The results shown in Figure 1D strongly suggest that CF-multi-S ($\tau > 4$ ms) and CF-multi-W ($\tau > 4$ ms) as well as CF-mono ($\tau > 4$ ms) have undergone dendritic translocation at P11–P14. However, it is possible that waveforms of qEPSCs are influenced by factors other than the locations of synapses, such as synaptic structure and the composition of individual postsynaptic receptors. Therefore, we examined more directly whether a higher incidence of slow qEPSCs reflects a higher degree of dendritic translocation of CFs. First, we estimated the 10%–90% rise times of qEPSCs arising from CF synaptic terminals on the PC soma. While recording from PCs innervated by CF-mono in mice at P11–P12, we applied a hypertonic sucrose solution locally to the PC soma from a glass micropipette in the presence of tetrodotoxin (0.5 μM), and evoked quantal release selectively from synaptic terminals around the PC soma (Figure S1). Frequency distribution of 10%–90% rise times of qEPSCs elicited by local sucrose application to the soma was almost identical to that of CF-multi-W ($\tau \leq 4$ ms), CF-mono ($\tau \leq 4$ ms), or CF-multi-S ($\tau \leq 4$ ms) (Figure S1). The average rise time of qEPSCs by somatic sucrose application (0.28 ± 0.02, mean ± SD, n = 6) did not differ from that for CF-multi-W ($\tau \leq 4$ ms), CF-mono ($\tau \leq 4$ ms), or CF-multi-S ($\tau \leq 4$ ms) ($p = 0.269$; ANOVA) (Table S2). These results suggest that the majority of qEPSCs following stimulation of these three types of CFs arose from synapses around the PC soma.

We then assessed whether 10%–90% rise times of qEPSCs are correlated with the extent of CF translocation to PC dendrites. For this purpose, we used transgenic mice expressing enhanced green fluorescent protein (EGFP) under the control of a serotonin receptor (Htr5b) promoter (Htr5b-EGFP mice). In these mice, EGFP is expressed in a subset of inferior olivery neurons, and CFs in the cerebellar cortex are sparsely EGFP positive (Figure 2A) (see Supplemental Experimental Procedures). We made whole-cell recordings from PCs whose stem dendrites were associated with single EGFP-positive CFs that appeared to have undergone dendritic translocation. First, we evoked CF-EPSCs arising from the strongest CF innervating the

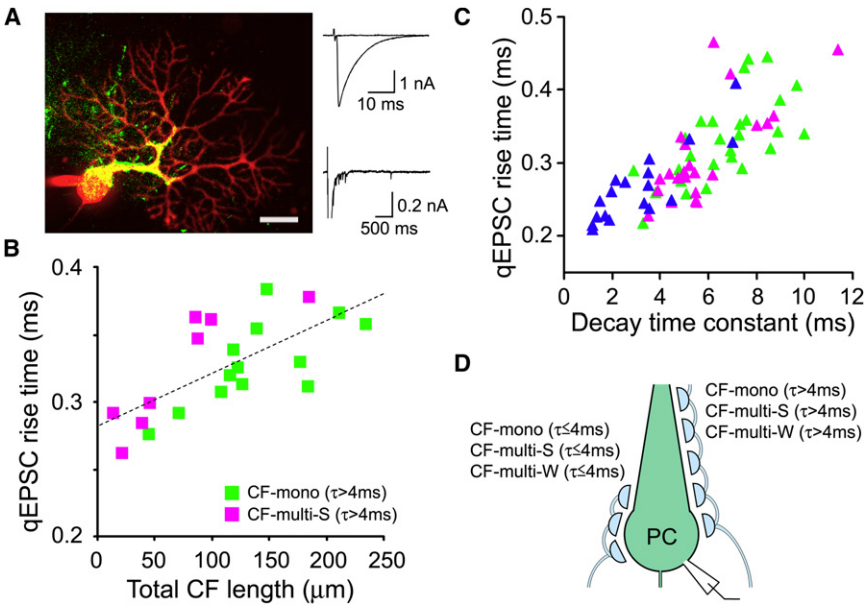

Figure 2. Innervation Patterns of PCs by CFs at P11–P14

(A) (Left) Merged confocal image for EGFP-positive CFs (green) and a patch-clamped PC filled with Alexa Fluor 568 (red). Note that the proximal dendrite of the PC was closely associated with an EGFP-positive CF (yellow). Scale bar, 20 μm. (Right) Representative traces of EPSCs evoked by stimulating the EGFP-positive CF at 0.2 Hz in the PC shown on the left. EPSCs were evoked at threshold stimulus intensity in normal Ringer solution (upper) and at suprathreshold intensity in the Sr^{2+}-containing solution (lower). Holding potential was –20 mV for the upper panel and −90 mV for the lower panel.

(B) The average 10%–90% rise time of qEPSCs is plotted against the total CF length. Data are from the experiments on Htr5b-EGFP mice as shown in (A). In these experiments, stimulated CFs were classified as either CF-mono ($\tau > 4$ ms) (n = 13, green boxes) or CF-multi-S ($\tau > 4$ ms) (n = 8, pink boxes).

(C) The average 10%–90% rise time of qEPSCs is plotted against the decay time constant of evoked CF-EPSCs. Data are from the same samples as in Figure 1D. Green, pink, and blue triangles represent CF-mono, CF-multi-S, and CF-multi-W, respectively.

(D) Schematic drawing of innervation patterns of CFs at P11–P14.

recorded PC (either CF-mono or CF-multi-S) by focal stimulation in the granule cell layer. We recorded qEPSCs arising from the strongest CF in the Sr^{2+}-containing external solution. Then, we moved the stimulation pipette and placed it at the tip of the EGFP-positive CF. In the normal external solution, we gradually increased the stimulus strength until the same "largest" CF-EPSC that was elicited by the granule cell layer stimulation appeared in an all-or-none fashion (Figures S2 and S3). This procedure confirmed that the EGFP-positive CF was the strongest CF innervating the recorded PC. In this experiment, all the CF-EPSCs elicited by the molecular layer stimulation had decay time constants longer than 4 ms. Thus, with this procedure, we could record EPSCs arising from CF-mono ($\tau > 4$ ms) or CF-multi-S ($\tau > 4$ ms) that extended along PC dendrites. We also measured the total CF length along the dendrites of each PC (Figure 2A). We found that the average 10%–90% rise time of qEPSCs was strongly correlated with the total CF length along PC dendrites ($r = 0.697$, $p = 0.0004$; Pearson's correlation coefficient test; Figure 2B). We also confirmed that the decay time constant of EPSCs, gathered by stimulating each CF (measured in normal external solution), was positively correlated with the total CF length ($r = 0.676$, $p = 0.0008$; Figure S4). These plots indicate that CFs that form terminals beneath the basal part of the primary dendrite are estimated to have 10%–90% rise times of qEPSCs shorter than 0.28 ms (i.e., the y intercept of the plot of Figure 2B) and decay time constants of evoked CF-EPSCs shorter than 4.8 ms (i.e., the y intercept of the plot of Figure S4). Furthermore, when the average 10%–90% rise time of qEPSCs originating from a CF (measured in Sr^{2+}-containing solution) was plotted against the decay time constant of EPSCs evoked by stimulating the same CF (measured in normal external solution), there was a strong correlation between the two parameters ($r = 0.774$, $p < 0.00001$; Figure 2C). Therefore, the extent of CF translocation can be estimated by the average 10%–90% rise times of qEPSCs as well as the analysis of the decay time constants of evoked CF-EPSCs.

The results shown in Figures 1D, 2B, and 2C collectively indicate that CF-EPSCs elicited by stimulating CF-mono ($\tau > 4$ ms), CF-multi-S ($\tau > 4$ ms), and CF-multi W ($\tau > 4$ ms) involve qEPSCs originating from PC dendrites much more so than those elicited by CF-mono ($\tau \leq 4$ ms), CF-multi-S ($\tau \leq 4$ ms), and CF-multi-W ($\tau \leq 4$ ms). Importantly, since CF-mono ($\tau > 4$ ms), CF-multi-S ($\tau > 4$ ms), and CF-multi-W ($\tau > 4$ ms) also involve qEPSCs with a fast rise time (≤0.2 ms, Figure 1D), they appear to have synapses around the PC soma. Thus, we assume that CF-multi-W ($\tau \leq 4$ ms), CF-multi-S ($\tau \leq 4$ ms), and CF-mono ($\tau \leq 4$ ms) form synapses around the soma, whereas CF-mono ($\tau > 4$ ms), CF-multi-S ($\tau > 4$ ms), and CF-multi-W ($\tau > 4$ ms) innervate both PC dendrites and somata (Figure 2D). It should be noted that at P11–P14, the majority of the strong CFs (CF-mono and CF-multi-S) had the decay time constants of their evoked EPSCs longer than 4 ms, whereas the majority of the weak CFs (CF-multi-W) had the decay time constants shorter than 4 ms (Figures 1A and 1B). Therefore, we conclude that at P11–P14, most of the strong CFs have undergone translocation to PC dendrites, whereas the majority of the weak CFs innervate soma and the most proximal portion of PC dendrites.

Because synapses from parallel fibers (PFs), the other excitatory inputs to PCs, are located at distal dendrites of PCs, rise times of qEPSCs arising from PFs are slow (Yamasaki et al., 2006). To estimate the possible contribution of PF-derived qEPSCs, we used a group III metabotropic glutamate receptor agonist, L-(+)-2-Amino-4-phosphonobutyric acid (L-AP4). Because L-AP4 is known to suppress PF-PC transmission without

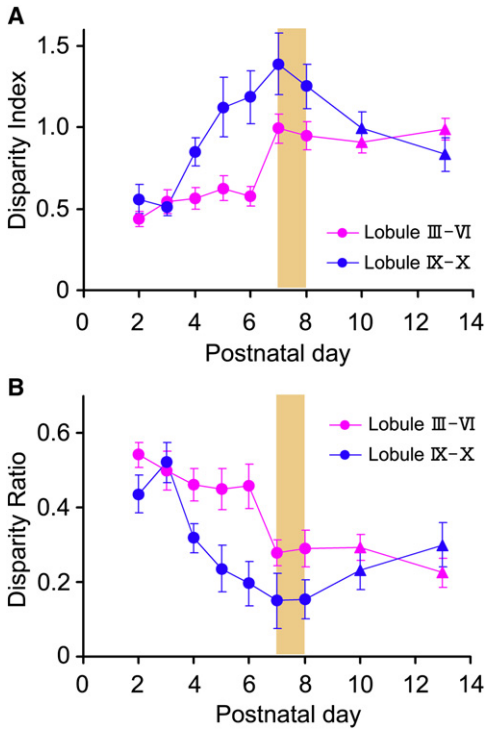

Figure 3. Functional Differentiation of CF Inputs Proceeds from Ventro-Caudal to Dorso-Rostral Lobules during Postnatal Cerebellar Development

(A and B) Developmental change in the Disparity Index (A) and the Disparity Ratio (B) for PCs sampled in lobules III–VI (pink) and lobules IX–X (blue). The number of PCs for each data point is 4–40. Data for P9–P11 and those for P12–P14 are pooled and plotted at P10 and P13 as triangles. Innervation patterns of CFs were analyzed in lobule III–VI just after the Disparity Index and the Disparity Ratio reached plateau levels (P7–P8; ocher area) in these lobules. Values are expressed as mean ± SEM.

appreciable effect on CF-PC transmission (Neale et al., 2001; Yamasaki et al., 2006), L-AP4 would significantly suppress qEPSCs with slow rise times, if PF-derived qEPSCs compose a substantial portion of qEPSCs following CF stimulation. However, L-AP4 (50 μM) caused no significant changes in the distribution of the 10%–90% rise time of qEPSCs following CF stimulation (Figure S5). This result clearly indicates that there was little, if any, contribution of PF-derived components in qEPSCs following CF stimulation.

Functional Differentiation of CFs into CF-multi-S and CF-multi-W Occurs on the PC Soma at P7–P8 before Initiation of CF Translocation

We next investigated the temporal relationship between CF translocation and functional differentiation of CF synapses. To clarify when functional differentiation of CF inputs occurred in lobules III–VI from which the PCs for the present analyses were sampled, we compared postnatal changes of the Disparity Index and Disparity Ratio in lobules III–VI with those in lobules IX–X (Figure 3). The Disparity Index represents variations of the amplitudes of EPSCs elicited by individual CF inputs, whereas the Disparity Ratio reflects the average of the inverse proportion of the strongest CF-EPSC amplitudes to each of the other weaker CF-EPSCs (Hashimoto and Kano, 2003) (see Supplemental Experimental Procedures). These parameters represent biased strengthening of one CF among multiple CFs innervating the same PC. Developmental changes in these parameters occurred earlier in the ventro-caudal part (lobules IX–X) than in the dorso-rostral part (lobules III–VI) (Figure 3). To examine CF innervation just after the completion of the functional differentiation of CFs into CF-multi-S and CF-multi-W, we confined our analyses to P7–P8 when the values of Disparity Index and Disparity Ratio just reached plateau levels in lobule III–VI (Figure 3).

At P7–P8, EPSCs for CF-multi-W had smaller amplitudes and faster decay time constants than those for CF-multi-S (Figures 4A and 4B), although the distinctions between the two populations were less clear (Figures 4A and 4B) and overall kinetics of CF-EPSCs tended to be slower in comparison with the data at P11–P14 (Table S1). We then estimated innervation patterns of CF-multi-S and CF-multi-W by analyzing rise times of qEPSCs (Figures 4C and 4D). Cumulative plots of the 10%–90% qEPSC rise times for CF-multi-S and CF-multi-W showed similar distributions (Figure 4D). The average 10%–90% rise times of qEPSCs were 0.27 ± 0.03 ms (n = 8) for CF-multi-S and 0.27 ± 0.03 ms (n = 10) for CF-multi-W with no significant difference (p = 0.787, t test). We further classified CF-multi-W into two subgroups at the decay time constant of 4 ms, whereas all of the CF-multi-S in our present experiment had decay time constants of evoked CF-EPSCs longer than 4 ms. We found that cumulative plots of the 10%–90% rise times of qEPSCs for CF-multi-W ($\tau \leq 4$ ms), CF-multi-W ($\tau > 4$ ms), and CF-multi-S were similar. The average 10%–90% rise times of qEPSCs were 0.27 ± 0.03 ms (n = 6) for CF-multi-W ($\tau \leq 4$ ms) and 0.27 ± 0.04 ms (n = 4) for CF-multi-W ($\tau > 4$ ms), with no significant difference from those of CF-multi-S (p = 0.945, ANOVA). In contrast to the result at P11–P14, the average 10%–90% rise time of qEPSCs did not correlate with the decay time constant of evoked CF-EPSCs (r = 0.146, p = 0.564) at P7–P8 (Figure 4E). These results indicate that at P7–P8, synapses arising from CF-multi-S and CF-multi-W are localized at sites with similar electrotonic lengths from the soma (Figure 4F). Therefore, functional differentiation of CFs into CF-multi-S and CF-multi-W occurs before the initiation of CF translocation to PC dendrites.

Translocation of Predominant CFs to PC Dendrites at P9–P10

To investigate when the difference in innervation patterns of CF-multi-S and CF-multi-W becomes evident, we followed developmental changes in the qEPSC rise time and the evoked CF-EPSC kinetics at every 2 postnatal days after P9. Since sample sizes of the minor populations of CF (CF-mono [$\tau \leq 4$ ms], CF-multi-S [$\tau \leq 4$ ms], and CF-multi-W [$\tau > 4$ ms]) were rather small (n = 1 or 2), we only plotted the data from the major populations of CF (CF-mono [$\tau > 4$ ms], CF-multi-S [$\tau > 4$ ms], and CF-multi-W [$\tau \leq 4$ ms]) in Figures 5B, 5C, 5E, 5F, 5H, and 5I. At P9–P10, EPSCs elicited by stimulating strong CFs (CF-mono and CF-multi-S) tended to have large amplitudes but relatively fast decay time constants (Figure 5A) when compared to those at P11–P12 (Figure 5D) and P13–P14 (Figure 5G). The incidences of qEPSCs with slow rise times were more frequent in CF-multi-S ($\tau > 4$ ms)

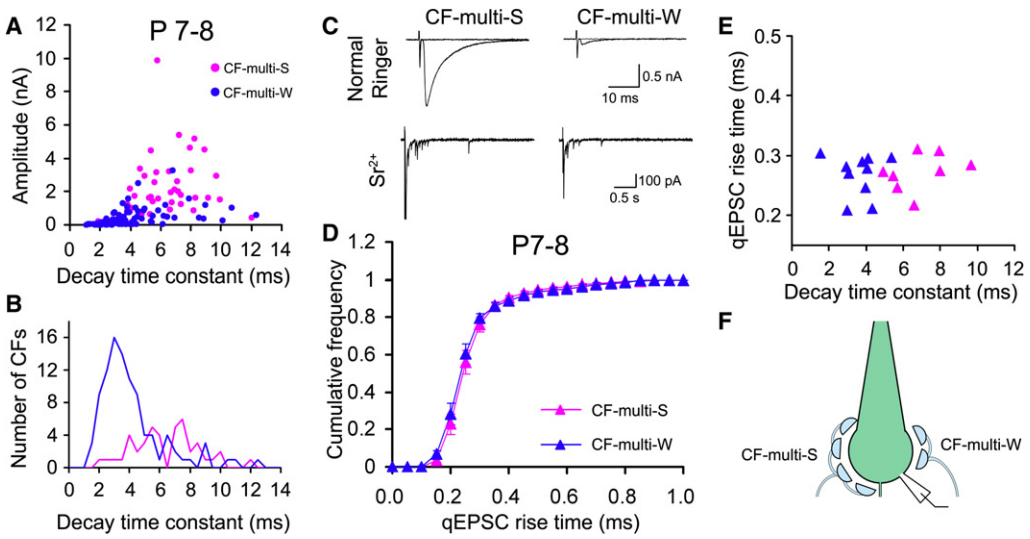

Figure 4. CF-EPSC Kinetics and Innervation Patterns of PCs by CFs at P7–P8

Histograms (A, B, D, and E) and sample CF-EPSC traces (C) are illustrated similarly to those in Figures 1 and 2 but for the data from mice at P7–P8. Sample numbers in (D) are n = 8 for CF-multi-S (pink) and n = 10 for CF-multi-W (blue). At this stage, synapses of CF-multi-S and CF-multi-W are considered to be located around the PC soma (F). Values are expressed as mean ± SEM.

than in CF-multi-W ($\tau \leq 4$ ms) (Figure 5B). Accordingly, the average qEPSC rise time for CF-multi-S ($\tau > 4$ ms) (0.27 ± 0.04 ms, n = 19) was significantly larger (p = 0.031, t test) than that for CF-multi-W ($\tau \leq 4$ ms) (0.24 ± 0.01 ms, n = 14), suggesting the initiation of CF translocation. However, the correlation between the qEPSC rise time and the CF-EPSC decay time constant was not very strong at this stage (r = 0.373, p = 0.023) (Figure 5C).

At P11–P12, data points representing CF-EPSC kinetics for CF-mono and CF-multi-S moved toward smaller amplitude and longer decay time constant (Figure 5D). Distinction between CF-multi-W and strong CFs (CF-mono and CF-multi-S) at the decay time constant of 4 ms became clear at this developmental stage. Simultaneously with the changes in decay time constant of evoked CF-EPSCs, differences in the cumulative frequencies of qEPSC rise times became larger between strong CFs (CF-mono [$\tau > 4$ ms] and CF-multi-S [$\tau > 4$ ms]) and weak CFs (CF-multi-W [$\tau \leq 4$ ms]) (Figure 5E). The average qEPSC rise time for CF-mono ($\tau > 4$ ms) (0.33 ± 0.06 ms, n = 9) was not significantly different from that for CF-multi-S ($\tau > 4$ ms) (0.30 ± 0.06 ms, n = 7, p > 0.05; Holm-Sidak test). In contrast, the average qEPSC rise time for CF-multi-W ($\tau \leq 4$ ms) (0.24 ± 0.02 ms, n = 6) was significantly smaller than that for CF-mono ($\tau > 4$ ms) (p < 0.05). The average qEPSC rise time became correlated with the decay time constant at P11–P12 (r = 0.739, p < 0.001) (Figure 5F). These trends became even clearer at P13–P14 (Figures 5G–5I). The average qEPSC rise time for CF-multi-W ($\tau \leq 4$ ms) (0.25 ± 0.03 ms, n = 8) was significantly shorter than that for CF-mono ($\tau > 4$ ms) (0.35 ± 0.05 ms, n = 15, p < 0.01; Holm-Sidak test), whereas the values were similar for CF-mono ($\tau > 4$ ms) and CF-multi-S ($\tau > 4$ ms) (p > 0.05). Importantly, the CF-EPSC kinetics and the qEPSC rise time for weak CFs remain almost unchanged from P9 to P14, whereas these parameters for strong CFs changed progressively during this period (Figure 5). These results suggest that innervation sites of strong CFs begin to shift from soma to dendrite at P9–P10 and that this change continues thereafter, whereas synapses arising from weak CFs remain around the PC soma throughout the developmental stage from P9 to P14.

Morphological Evidence for Translocation of Single CF to PC Dendrites

Next we employed neuroanatomical techniques to pursue the developmental profile of CF innervation. First, we followed the transition from the "pericellular nest" stage to the "peridendritic" stage of CF innervation by labeling CFs with the anterograde tracer biotinylated dextran amine (BDA) and immunostaining PCs with an antibody against calbindin (Figure 6). Pericellular nests with extensive branching of CFs around PC somata were observed at P7, P9, and P12, being most conspicuous at P9 (Figures 6A–6C and 6H–6J). At P7, CFs innervated PC somata, despite the presence of immature PC dendrites that were short in length and poor in branching (Figures 6A and 6H). Dendritic innervation started at P9, when CF innervation was confined to the basal portion of PC dendrites (Figures 6B and 6I). At P12 and thereafter, the territory of CF innervation extended progressively along PC dendrites following the elongation of dendritic arbors (Figures 6C, 6D, 6E, and 6J). The developmental extension of CF innervation territory was quantified by measuring the length from the apical pole of PC somata to the tips of tracer-labeled CFs (Figure 6F) and its relative height in the molecular layer (Figure 6G). These results indicate that pericellular nests disappear during P9–P15, whereas dendritic translocation of CF innervation is a more protracted process that starts at P9 and continues at least until P20.

During the developmental stage of the pericellular nest (~P12), this structure emitted a number of collateral branches, which traversed rostrocaudally in parasagittal cerebellar sections and formed varicosities along the base of dendrites and the somata

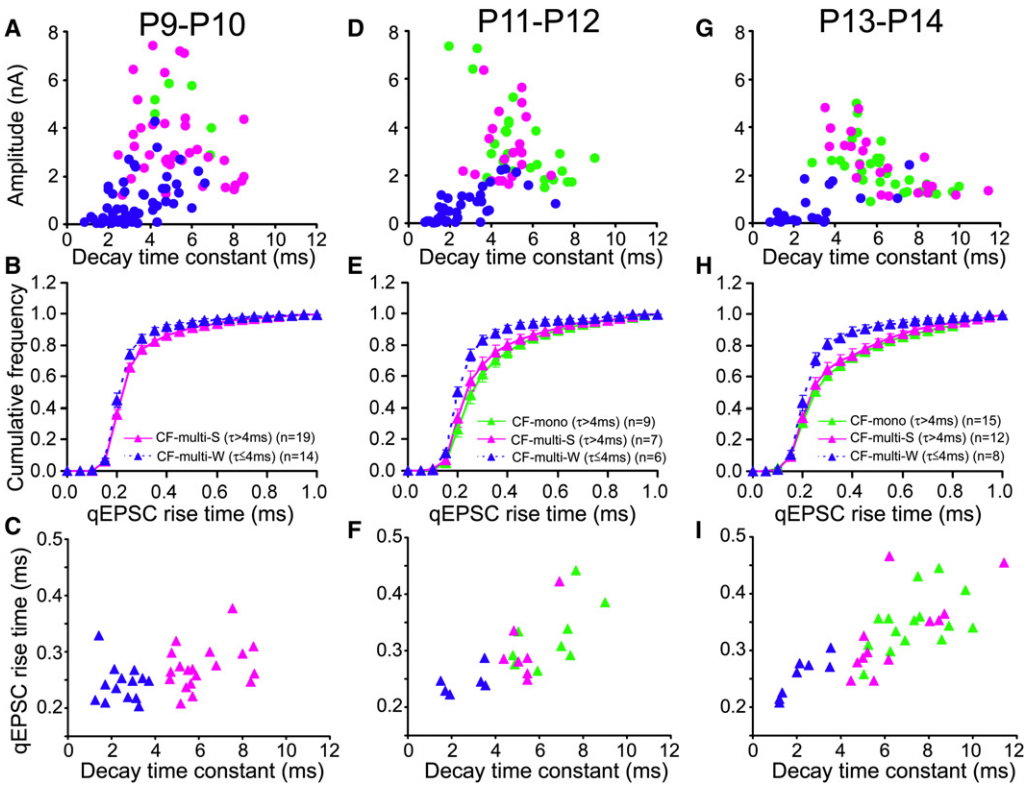

Figure 5. Postnatal Changes in CF Innervation Patterns

(A, D, and G) The CF-EPSC amplitude is plotted against the decay time constant. Data were sampled in lobule III–VI at P9–P10 (A), P11–P12 (D), and P13–P14 (G). Green, pink, and blue symbols represent CF-mono, CF-multi-S, and CF-multi-W, respectively. (B, E, and H) Average cumulative histograms for the 10%–90% rise times of qEPSCs recorded at P9–P10 (B), P11–P12 (E), and P13–P14 (H). Green, pink, and blue symbols represent CF-mono ($\tau > 4$ ms), CF-multi-S ($\tau > 4$ ms), and CF-multi-W ($\tau \leq 4$ ms), respectively. (C, F, and I) The average 10%–90% rise time of qEPSCs is plotted against the decay time constant of evoked CF-EPSCs. Plotted data are sampled at P9–P10 (C), P11–P12 (F), and P13–P14 (I). Correlation coefficient was 0.373 ($p = 0.023$) at P9–P10, 0.739 ($p < 0.0001$) at P11–P12, and 0.775 ($p < 0.0001$) at P13–P14. Values are expressed as mean ± SEM.

of neighboring PCs (single arrowheads in Figures 6A–6C and 6H–6J). This data suggests that the pericellular nest is composed of branches of predominant CFs and axon collaterals arising from the CFs innervating the neighboring PCs. At P15 when typical pericellular nests were no longer seen, CFs ascended the PC layer without emitting collateral branches, and occasionally formed a few terminal-like swellings on the apical half of the PC soma (Figure 6D). At P20, such perisomatic CF terminals became very rare (Figure 6E). These results raise an intriguing possibility that the loss of pericellular nests represents pruning of CF collaterals and establishment of monoinnervation of PCs.

Accomplishment of Single CF Innervation by Elimination of CF Synapses on the Soma and the Basal Portion of Primary Dendrites of PCs

To test the aforementioned possibility, we employed double labeling of CFs with the anterograde tracer BDA and an antibody against type 2 vesicular glutamate transporter (VGluT2) at P9 (Figures 7A–7E), P12 (Figures 7F–7L and S6), and P15 (Figure S7). For the serial electron microscopic analysis, we examined, at each developmental stage, three PCs that were innervated densely by tracer-labeled CFs. Although VGluT2 was expressed in both CF and PF terminals during early postnatal development (Miyazaki et al., 2003), they could be distinguished morphologically. CF terminals were identified as large perisomatic/peridendritic puncta, while PF terminals were small neuropil puncta (Figures 7A and 7F).

At P9, calbindin-labeled PC somata were surrounded and contacted by CFs that were double labeled for BDA and VGluT2 (*d-CF*, yellow puncta) and by CFs that were labeled for VGluT2 alone (*s-CF*, green puncta) (Figure 7A). This observation was substantiated by reconstruction of serial electron microscopic sections (Figures 7B–7E). Some somatic spines formed asymmetrical synapses with CF terminals that were labeled for both BDA (diffuse DAB labeling) and VGluT2 (metal particles) (*d-CF*, Figures 7B, 7C and 7E), while other spines of the same PCs formed asymmetrical synapses with CF terminals that were labeled for VGluT2 alone (*s-CF*, Figures 7B–7D). In all of the three PCs examined, mixed innervation by *d-CF* and *s-CF* was confirmed at somata and at the basal portion of dendrites (Figure 8A).

At P12, somata of PCs were contacted by both *d-CF* and *s-CF*, whereas proximal shaft dendrites were exclusively associated with *d-CF* (Figure 7F). In all of the 20 PCs analyzed by multiple fluorescent labeling, single predominant CFs displayed dendritic translocation, whereas lesser CFs remained within the somatic and basal dendritic compartments (Figure S6). Electron

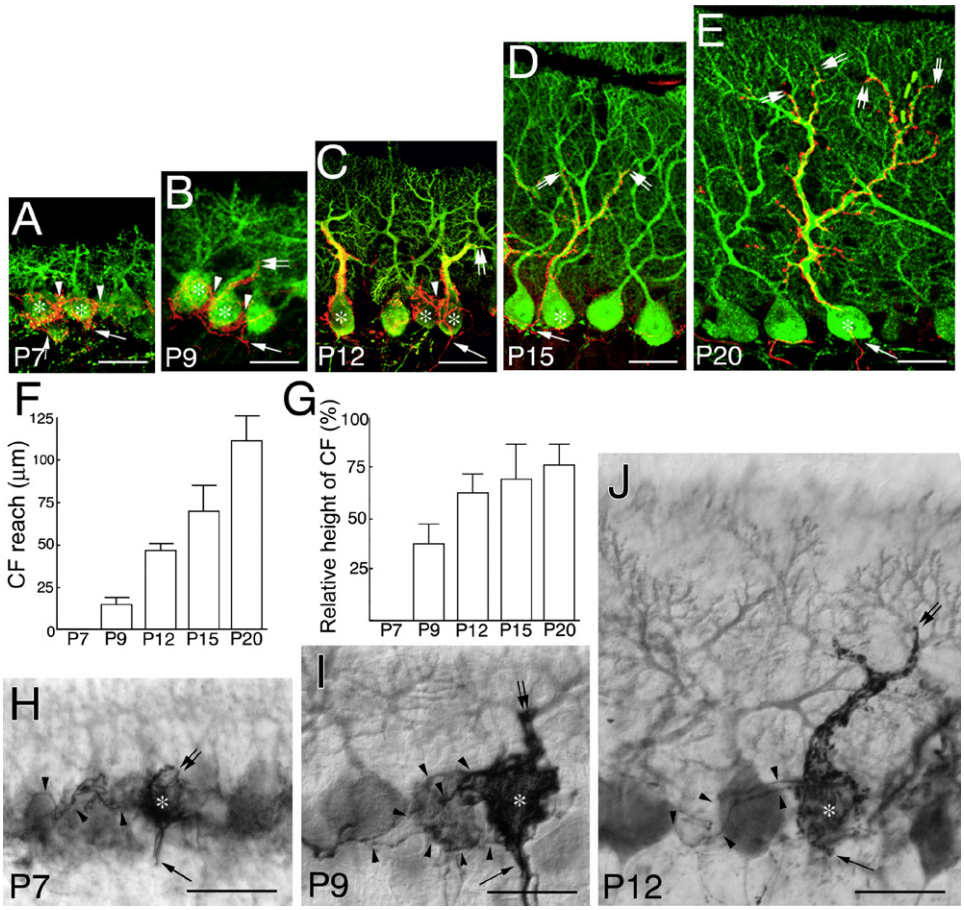

Figure 6. Developmental Profile of CF Innervation from Perisomatic Nest Stage to Peridendritic Stage

(A–E) Fluorescent labeling of CFs with BDA (red) and PCs with calbindin antibody (green) at P7 (A), P9 (B), P12 (C), P15 (D), and P20 (E).

(F and G) Developmental changes in the mean height of CF reach (F) and its relative height in the molecular layer (G). Values are mean ± SD for 10 to 12 CFs labeled with BDA from three mice at each age. CF reach was measured from the apical pole of PC somata to the tips of tracer-labeled CFs.

(H–J) Dark labeling of CFs with BDA (DAB/cobalt) and pale labeling of PCs with calbindin antibody (DAB) at P7 (H), P9 (I), and P12 (J). Arrows and double arrows indicate CFs reaching the PC layer and their tips in the molecular layer, respectively. Arrowheads indicate CF collaterals projecting to neighboring PCs. Asterisks indicate PC somata innervated densely by tracer-labeled CFs. Scale bars, 20 μm.

microscopic examination confirmed this pattern of innervation (Figures 7G–7L and 8B). These morphological results support our electrophysiological data that a single CF undergoes dendritic translocation in the majority of PCs.

At P15, somatic innervation by CFs became rare, and dendrites were innervated by *d-CF* only (Figures S7 and 8C). From the reconstructed data, the density and composition of CF synapses were quantitatively evaluated. The density of somatic CF synapses (per 1 μm of CF height) decreased progressively from P9 to P15 (Figure 8D). When similar assessment was applied to dendritic portions, the density of dendritic CF synapses (per 1 μm of CF height) peaked at P12 with substantial reduction at P15 (Figure 8F). The composition of somatic synapses formed by *d-CF* was 54%–57% at P9 and P12, and reached 100% at P15, although the somatic synapses were very few at P15 (Figure 8E). On the other hand, the composition of dendritic synapses formed by *d-CF* was as high as 91% at P9, transiently reduced to 75% at P12, and reached 100% at P15 (Figure 8G).

Taken together, these anatomical findings indicate that pericellular nests do represent multiple innervation of PCs by CFs with different neuronal origins. Multiple CFs innervating each PC exhibit different extents of dendritic translocation at P12. A main CF extends progressively toward the transition points between proximal and distal dendrites, whereas innervation territories of the lesser CFs are confined below the basal portion of the proximal dendrites. Subsequently, the monoinnervation pattern of CF wiring is achieved around P15 by the elimination of synapses of the lesser CFs from the soma and basal dendrites.

DISCUSSION

Functional Strengthening of a Single CF on the PC Soma Precedes Translocation of a Predominant CF to PC Dendrites

Our electrophysiological analyses demonstrated that the distribution of qEPSC rise times was identical between CF-multi-S

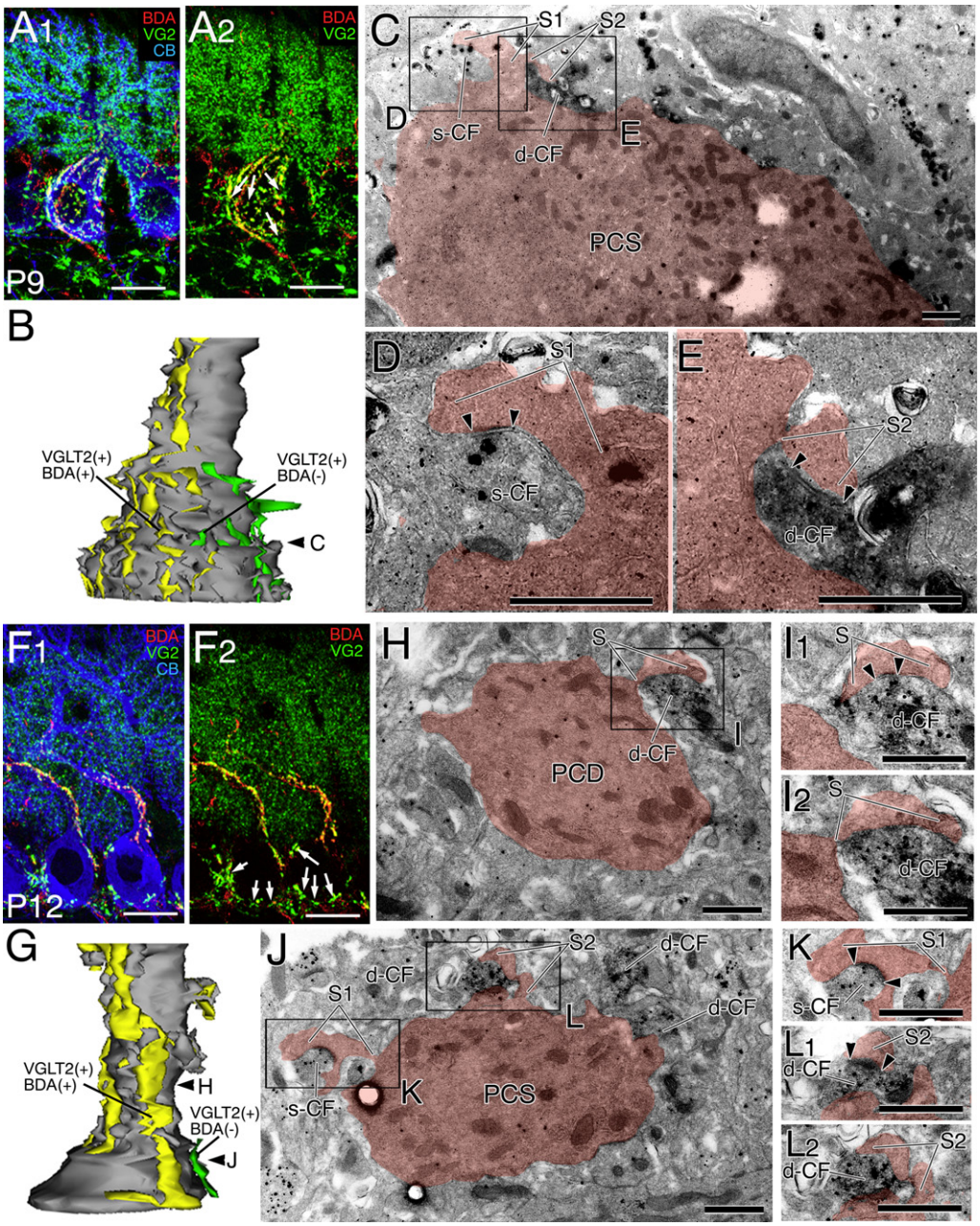

Figure 7. Double Labeling of CFs with the Anterograde Tracer BDA and the VGluT2 Antibody at P9 and P12

(A and F) Triple fluorescent labeling for BDA (red), VGluT2 (VG2, green), and a PC marker, calbindin (CB, blue). (B and G) 3D reconstructed images of innervation by *d-CF* labeled for BDA and VGluT2 (yellow) and *s-CF* labeled for VGluT2 alone (green). Arrowheads attached to the reconstructed images indicate the levels of PC dendrite at which the cross-sections of electron micrographs shown in (C), (H), and (J) were obtained. (C–E and H–L) Electron micrographs show that spines (S) from the PC soma (PCS) at P9 and P12 are innervated by both *s-CF* (D and K) and *d-CF* (E and L), whereas those from PC dendrites (PCD) at P12 are exclusively innervated by *d-CF* (I). Boxed regions in (C), (H), and (J) are enlarged in (D) and (E), (I), and (K) and (L), respectively. Scale bars: (A) and (F), 10 μm; (C–E) and (H–L), 1 μm. Arrows indicate CF terminals labeled for VGluT2 alone. Arrowheads indicate synaptic contact sites.

and CF-multi-W at P7–P8, but the fraction of qEPSCs with slow rise times increased for CF-multi-S and CF-mono after P9–P10 (Figures 5B, 5E, and 5H). In contrast to CF-multi-S and CF-mono, the distribution of qEPSC rise times of most CF-multi-Ws did not change from P9 to P14 (Figures 5B, 5E, and 5H). Our morphological analyses revealed that all CFs initially had synapses around the PC soma, and in the majority of PCs, single CFs extended along dendrites and formed synaptic contacts at P9–P12 (Figures 6 and 8). Synaptic terminals of the other CFs were confined beneath the basal part of primary dendrites

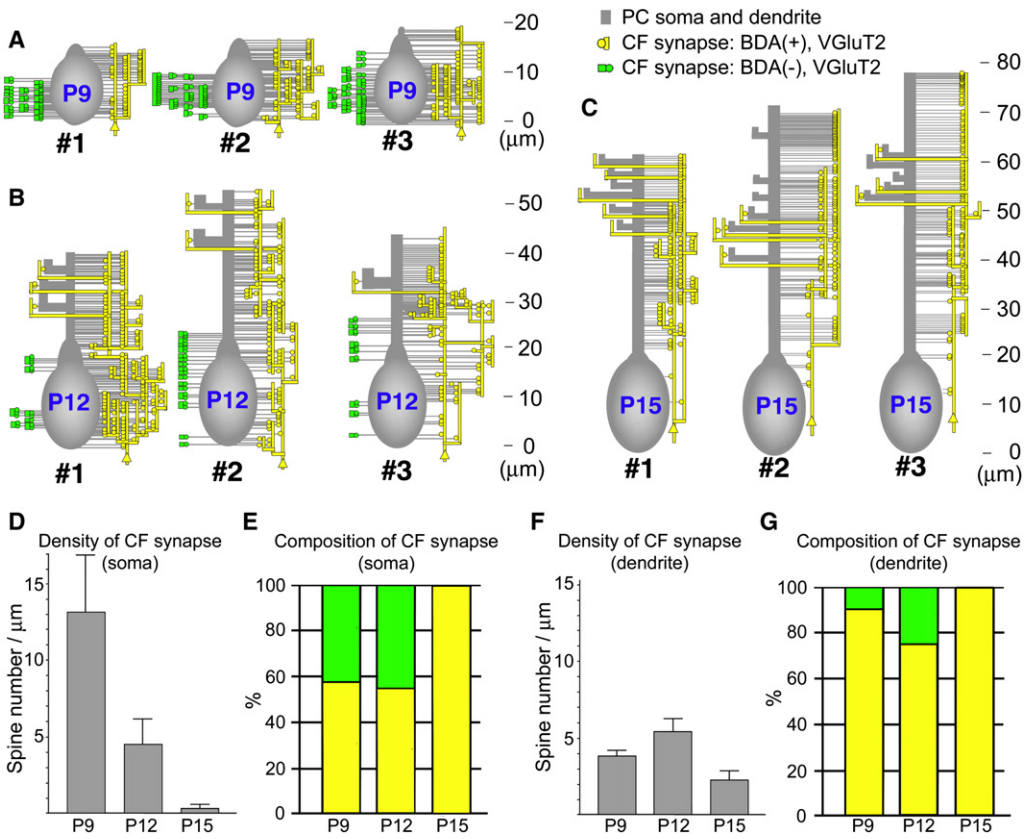

Figure 8. Schematic Representation and Quantitative Assessment of CF Wiring onto PC Somata and Dendrites at P9, P12, and P15

(A–C) Three PCs each were reconstructed from serial electron microscopy at P9 (A), P12 (B), and P15 (C). Yellow lines and circles on the right side of each PC represent *d-CF* labeled for BDA and VGluT2, while green circles on the left side represent *s-CF* labeled for VGluT2 alone. Note that pericellular nests formed by *d-CF* progressively undergo translocation to dendrites with age, whereas those formed by *s-CF* are confined to the soma and basal dendrites at P9 and P12, and are eventually ablated at P15. Scales to the right show the height from the base of the PC soma. (D and F) Density of CF synapses in the soma (D) and dendrites (F) expressed as the number of synapses per 1 μm of CF height. Values are mean ± SD. (E and G) Composition of synapses by *d-CF* (yellow) and *s-CF* (green) in the soma (E) and dendrites (G).

(Figure 8B). Thus, these electrophysiological and morphological data collectively indicate that single CFs that elicit the largest CF-EPSCs extend their synapses along PC dendrites at P9–P12, whereas synapses from the other CFs that induce smaller CF-EPSCs remain around the PC soma.

We also found that CF translocation started at P9 after the completion of selective strengthening of a single CF among multiple CFs innervating the same PC (Figures 3, 4, and 5). Competition among multiple CFs occurs on the PC soma, and then only the strengthened CF appears to extend its innervation to dendrites in the majority of PCs. The expansion of CF innervation territory continues until CF monoinnervation is established around P20. Therefore, the results of the present study suggest that selective strengthening of a single CF on the PC soma may be an important process for selecting the single CF that presumably innervates that PC throughout life. However, the strengthened synapse at an early stage of postnatal development may not necessarily become the winner in the mature nervous system, as shown in the neuromuscular junction (Walsh and Lichtman, 2003). Our previous results indicate that CF-multi-W with a Disparity Ratio smaller than 0.2 is preferentially eliminated within 2 days (Hashimoto and Kano, 2003), suggesting that weaker CFs will eventually be eliminated. Future studies with time-lapse imaging of the same CFs over days during the period of CF translocation might elucidate whether the strengthened CF on the PC soma around P7 eventually becomes the single remaining CF.

The results of the present study suggest that morphological changes in CF synapses around the PC soma underlie selective strengthening of a single CF. Our serial electron-microscopic data demonstrated that more than half of CF synaptic terminals on the PC soma (57%) were formed by a single predominant CF at P9 (Figure 8E, *d-CF*). Since the other CFs form synapses on the PC soma, the rest of the somatic CF synapses (43%) should be supplied by the lesser CFs. Since the mean number of CFs observed in individual, multiply innervated PCs is 3.5 at P9 (i.e., each PC is innervated by one predominant CF and 2.5 lesser CFs on average), it follows that each lesser CF supplies 17% of somatic CF synapses on average. Therefore, the strength of a lesser CF should be about 1/3 of that of the predominant CF. This value roughly corresponds to the Disparity Ratio estimated by our electrophysiological analysis (Figure 3). Sugihara (2005)

demonstrates that CF innervation pattern in the PC layer is rearranged from "loose creeper type" to "dense nest type" during P4–P7 in rat, which corresponds to the postnatal period in mice when CF functional differentiation occurs (Hashimoto and Kano, 2003). These results suggest that functional differentiation of multiple CF inputs during P4–P7 is based mainly on the increase in the number of synaptic terminals supplied by each CF on the PC soma.

We found that minor portions of strong CFs with decay time constants shorter than 4 ms (11.1% [n = 27] for CF-mono [$\tau \leq$ 4 ms], 13.6% [n = 22] for CF-multi-S [$\tau \leq 4$ ms]) showed qEPSC distributions similar to CF-multi-W ($\tau \leq 4$ ms) at P11–P14 (Figure 1D). This result indicates that such strong CFs have not extended their synapses along dendrites at this age. Conversely, we also found that a relatively minor portion of weak CFs with decay time constants longer than 4 ms (22.2% [n = 18] for CF-multi-W [$\tau > 4$ ms]) showed a qEPSC distribution similar to CF-mono ($\tau > 4$ ms) and CF-multi-S ($\tau > 4$ ms) at P11–P14 (Figure 1D). This result indicates that at least in such cases, multiple CFs undergo translocation to PC dendrites, as suggested previously by Na^+ imaging technique (Scelfo et al., 2003). However, multiple CF translocation has not been reported in previous morphological studies (Bravin et al., 1995; Miyazaki et al., 2004). Moreover, we could not obtain any morphological evidence for multiple CF translocation in the developing cerebellum (Figures 6, 7, 8, and S6). Our previous investigation of innervation sites of multiple CFs by using a Ca^{2+} indicator also suggested that the weak CFs formed terminals at the basal part of PC dendrites and around the PC soma at P10–P14 (Hashimoto and Kano, 2003). We assume that PCs with multiple CF translocation may be so rare that previous morphological and Ca^{2+} imaging analyses failed to detect such cases. In contrast, the previous data for multiple CF translocation based on imaging of Na^+ influx during CF-EPSCs (Scelfo et al., 2003) might be an overestimate, because Na^+ easily diffuses from the site of entry within cytoplasm (Callaway and Ross, 1997; Knopfel et al., 2000) and, therefore, it is difficult to estimate the precise location of CF synapses from the Na^+ signals. In the present study, the percentage of PCs innervated by both CF-multi-S ($\tau > 4$ ms) and CF-multi-W ($\tau > 4$ ms), which presumably represents translocation of multiple CFs, was only 7.1% of PCs (n = 98) that were used for the CF waveform analysis at P11–P14 (Figure 1A). Therefore, we conclude that only the strongest CF can undergo translocation to dendrites in the majority of PCs.

Maturation of CF Synaptic Transmission Also Contributes to Functional Differentiation of CFs

At P11–P14, the degree of CF translocation estimated by the decay time constants of evoked CF-EPSCs and the rise times of qEPSCs correlated well with the morphological data (Figures 1, 6, and 8). At P7–P8, however, there was no clear correlation between the two electrophysiological parameters (Figure 4E). Although both morphological data and qEPSC rise times indicated that nearly all CF synapses were present around the PC soma, the decay time constants of EPSCs from CF-multi-S were significantly longer than those from CF-multi-W (Figures 4, 6, and 8). This is because the decay time constants of evoked CF-EPSCs can be affected by factors other than dendritic filtering. At P7–P8, the 10%–90% rise times (Figure 4D) and decay time constants (CF-multi-S, 1.38 ± 0.26 ms; CF-multi-W, 1.23 ± 0.25 ms, p = 0.203; t test) of qEPSCs resulting from CF-multi-S and CF-multi-W were not significantly different. This result suggests presynaptic origin of the slow decay time constant of evoked CF-EPSCs, such as asynchronous vesicle release and/or delayed clearance of glutamate. We have demonstrated previously that the pattern of transmitter release changes from "one-site one-vesicle release" to "multivesicular release" at strong CFs during postnatal development (Hashimoto and Kano, 2003). Because multivesicular release results in the larger glutamate transients at synaptic clefts, the delay of transmitter clearance and/or spillover to extrasynaptic AMPA receptors might prolong the decay of the predominant CF-EPSCs (Wadiche and Jahr, 2001). Therefore, not only the increase in the number of synaptic terminals per CF but also the maturation of CF synaptic transmission contributes to functional differentiation of CFs.

Pericellular Nests Represent Multiple CF Innervation of PCs

Ramón y Cajal (1911) described the development of CFs in three successive stages: (1) a pericellular nest stage during which CFs establish their contact with PCs by forming a plexus on the lower part of the PC somata, (2) a "capuchon" stage characterized by the displacement of the plexus to the apical portion of PC somata and main dendrites with somatic nature, and (3) a "dendritic" stage in which CFs spread upwards into dendrites (Ramón y Cajal, 1911). The pericellular nest and capuchon stages correspond to P6–P9 in mice, where CFs innervate numerous spine-like structures protruding from PC somata and immature basal dendrites (Altman, 1972; Kiyohara et al., 2003; Larramendi, 1969). We confirmed this result in our morphological observations of mice at P7 and P9. Our finding of CF collaterals projecting to adjacent PCs is also consistent with previous studies (Marin-Padilla, 1985; Mason et al., 1990; Mason and Gregory, 1984). Furthermore, the completion of CF translocation to dendrites around P15 (the dendritic stage) agrees with an anatomical study in rats (Chedotal and Sotelo, 1992). Therefore, the stage and mode of CF translocation found in the present study correspond well with those reported previously. By applying double labeling of CFs with anterograde tracer and VGluT2 antibody to light and electron microscopic analyses, we have disclosed that pericellular nests do represent multiple CF innervation of PCs, and that a single main CF extends progressively toward distal spiny branchlets with other surplus CFs remaining around the soma and the basal portion of dendrites. Our morphological data clearly show that the pericellular nests consist of synapses of a single predominant CF undergoing translocation to dendrites and those of lesser CFs that are collaterals of predominant CFs to adjacent PCs.

The PC soma was associated with the CF terminals at P12, but they were removed by P15 together with surplus CFs (Figures 6C, 6D, 8B, 8C, and 8D). At the same time, predominant CFs that had extended to dendrites also lost their terminals from the soma (Figures 8B and 8C). Therefore, the CF synapse elimination during this postnatal period removes CF synaptic terminals around the PC soma without affecting synapses of

predominant CFs on dendrites. These results suggest that the elimination process is rather nonselective. Surplus CFs are almost completely eliminated by P15 because their synapses are confined to the PC soma. This elimination signal appears to be dependent on neural activity along the mossy fiber-granule cell-PF-PC pathway involving NMDA receptors at mossy-fiber-to-granule-cell synapses (Kakizawa et al., 2000) and type 1 metabotropic glutamate receptor and its downstream signaling within PCs (Hashimoto and Kano, 2005; Ichise et al., 2000; Kano et al., 1995, 1997, 1998; Offermanns et al., 1997). In contrast, the predominant CFs can escape from this elimination signal and survive because they innervate PC dendrites. Therefore, the selectivity of CF synapse elimination appears to be determined by the selective translocation of single CFs to PC dendrites.

EXPERIMENTAL PROCEDURES

Electrophysiological Analyses

All experiments were conducted according to the guidelines of the Animal Welfare Committees of Osaka University, Sapporo Medical University, Hokkaido University, and The University of Tokyo. Parasagittal cerebellar slices (250 μm thickness) were prepared from C57BL/6 mice at P7 to P14 or from Htr5b-EGFP mice at P9 to P14 as described previously (Edwards et al., 1989; Hashimoto and Kano, 2003). The Htr5b-EGFP mice (*Egfp*-BAC transgenic mice [*Tg(Htr5b-EGFP)1Gsat/Mmmh*]), which were generated by the Gene Expression Nervous System Atlas (GENSAT) Project (Gong et al., 2003), were obtained from Mutant Mouse Regional Resource Centers (MMRRC).

Whole-cell recordings were made from visually identified PC somata using an upright microscope (BX50WI or BX51WI, Olympus, Tokyo, Japan). All experiments were carried out at 31°C. Resistances of patch pipettes were 2–3 MΩ when filled with an intracellular solution composed of (in mM) 60 CsCl, 10 Cs D-gluconate, 20 TEA-Cl, 20 BAPTA, 4 $MgCl_2$, 4 ATP, and 30 HEPES (pH 7.3, adjusted with CsOH). The pipette access resistance was compensated by 70%–80%. The composition of the standard bathing solution was (in mM) 125 NaCl, 2.5 KCl, 2 $CaCl_2$, 1 $MgSO_4$, 1.25 NaH_2PO_4, 26 $NaHCO_3$, and 20 glucose, bubbled with 95% O_2 and 5% CO_2. Bicuculline (10 μM) was always added to block inhibitory synaptic transmission. Ionic currents were recorded with an Axopatch 1D (Molecular Devises, Sunnyvale, CA) or EPC-10 (HEKA, Lambrecht/Pfalz, Germany) patch-clamp amplifier. The signals were filtered at 3 kHz and digitized at 20 kHz for recording evoked EPSCs. Online data acquisition and offline data analysis were performed using PULSE software (HEKA). Stimulation pipettes (5–10 μm tip diameter) were filled with standard saline. Stimuli (duration, 0.1 ms; amplitude, 0–90 V) were applied at 0.2 Hz. CFs were stimulated in the granule cell layer 50–100 μm away from the PC soma. The number of CFs innervating the recorded PC was estimated from the number of discrete CF-EPSC steps. To record quantal CF-EPSCs, external 2 mM Ca^{2+}/1 mM Mg^{2+} was replaced with 1 mM Sr^{2+}/2 mM Mg^{2+} or 5 mM Sr^{2+}/1 mM Mg^{2+}. The signals were digitized and sampled at 40 kHz. qEPSCs were analyzed by Mini Analysis Program (ver. 5.1.1, Synaptosoft Inc., Decatur, GA).

SigmaStat (ver. 3.11 Systat Software Inc., Chicago, IL) was used for statistical analysis. Statistical significance was determined with t tests and ANOVA. Holm-Sidak test was used for post hoc analysis. Data in the text are expressed as mean ± SD.

Morphological Analyses

Under anesthesia with chloral hydrate (350 mg/kg of body weight, i.p.), a glass pipette filled with 2–3 μl of 10% solution of BDA (10,000 MW, Invitrogen, Carlsbad, CA) in phosphate-buffered saline (pH 7.4) was inserted stereotaxically to the inferior olive by the dorsal approach. The tracer was injected iontophoretically by applying square positive current pulses (7 μA, 700 ms) at 0.5 Hz for 15 min. After 3 days of survival, mice were anesthetized and fixed by transcardial perfusion with 0.1% glutaraldehyde and 4% paraformaldehyde in 0.1M sodium phosphate buffer (pH 7.2). The straight portion of lobules IV–V was analyzed.

For bright-field light microscopy, CFs were visualized with streptavidin-peroxidase conjugate and stained black by using DAB and cobalt. PCs were labeled with brown DAB products by immunoperoxidase reaction for calbindin (Nakagawa et al., 1998). For immunofluorescence, sections were incubated with rabbit calbindin antiserum or with a mixture of rabbit calbindin antiserum and goat VGluT2 antibody (Miura et al., 2006), followed by 2 hr incubation with a mixture of fluorophore-linked streptavidin and secondary antibodies. Images were taken with a confocal laser scanning microscope (R2100Ag2, BioRad, Herculues, CA).

For electron microscopy, BDA-labeled sections were incubated overnight with guinea pig VGluT2 antibody and avidin-biotin-peroxidase complex. Then, sections were incubated with 1.4 nm gold-particle-conjugated anti-guinea pig antibody (1:200, Nanogold, Nanoprobes, Stony Brook, NY) for 3 hr. Immunogold for VGluT2 was first silver-enhanced using an HQ-silver enhance kit (Nanoprobes), and then BDA was visualized with DAB. Serial ultrathin sections were prepared in the plane parallel to the pial surface. 3D reconstructed images were built using free software package (*Reconstruction*) developed by Kristen Harris and John Fiala (available at Synapse Web [http://synapses.clm.utexas.edu/tools/reconstruct/reconstruct.stm]).

SUPPLEMENTAL DATA

Supplemental data for this article include Supplemental Experimental Procedures, seven figures, and two tables and can be found at http://www.cell.com/neuron/supplemental/S0896-6273(09)00461-9.

ACKNOWLEDGMENTS

This work was supported by Grants-in-Aid for Scientific Research (17023021 and 17100004 to M.K., and 17023001 to M.W.) from the Ministry of Education, Science, Sports, Culture, and Technology of Japan. This work was also supported by Takeda Science Foundation (K.H.).

Accepted: June 4, 2009
Published: July 15, 2009

REFERENCES

Altman, J. (1972). Postnatal development of the cerebellar cortex in the rat. II. Phases in the maturation of Purkinje cells and of the molecular layer. J. Comp. Neurol. *145*, 399–463.

Altman, J., and Bayer, S.A. (1997). Development of the Cerebellar System: In Relation to Its Evolution, Structure, and Functions (Boca Raton, FL: CRC Press).

Bravin, M., Rossi, F., and Strata, P. (1995). Different climbing fibres innervate separate dendritic regions of the same Purkinje cell in hypogranular cerebellum. J. Comp. Neurol. *357*, 395–407.

Callaway, J.C., and Ross, W.N. (1997). Spatial distribution of synaptically activated sodium concentration changes in cerebellar Purkinje neurons. J. Neurophysiol. *77*, 145–152.

Chedotal, A., and Sotelo, C. (1992). Early Development of Olivocerebellar Projections in the Fetal Rat Using CGRP Immunocytochemistry. Eur. J. Neurosci. *4*, 1159–1179.

Crepel, F. (1982). Regression of functional synapses in the immature mammalian cerebellum. Trends Neurosci. *5*, 266–269.

Edmonds, B., Gibb, A.J., and Colquhoun, D. (1995). Mechanisms of activation of glutamate receptors and the time course of excitatory synaptic currents. Annu. Rev. Physiol. *57*, 495–519.

Edwards, F.A., Konnerth, A., Sakmann, B., and Takahashi, T. (1989). A thin slice preparation for patch clamp recordings from neurones of the mammalian central nervous system. Pflüger Arch. *414*, 600–612.

Gong, S., Zheng, C., Doughty, M.L., Losos, K., Didkovsky, N., Schambra, U.B., Nowak, N.J., Joyner, A., Leblanc, G., Hatten, M.E., and Heintz, N. (2003).

A gene expression atlas of the central nervous system based on bacterial artificial chromosomes. Nature *425*, 917–925.

Hashimoto, K., and Kano, M. (2003). Functional differentiation of multiple climbing fiber inputs during synapse elimination in the developing cerebellum. Neuron *38*, 785–796.

Hashimoto, K., and Kano, M. (2005). Postnatal development and synapse elimination of climbing fiber to Purkinje cell projection in the cerebellum. Neurosci. Res. *53*, 221–228.

Hashimoto, K., Ichikawa, R., Takechi, H., Inoue, Y., Aiba, A., Sakimura, K., Mishina, M., Hashikawa, T., Konnerth, A., Watanabe, M., and Kano, M. (2001). Roles of glutamate receptor δ2 subunit (GluRδ2) and metabotropic glutamate receptor subtype 1 (mGluR1) in climbing fiber synapse elimination during postnatal cerebellar development. J. Neurosci. *21*, 9701–9712.

Hashimoto, K., Yoshida, T., Sakimura, K., Mishina, M., Watanabe, M., and Kano, M. (2009). Influence of parallel fiber-Purkinje cell synapse formation on postnatal development of climbing fiber-Purkinje cell synapses in the cerebellum. Neuroscience, in press. Published online December 3, 2008. 10.1016/j.neuroscience.2008.12.037.

Hensch, T.K. (2004). Critical period regulation. Annu. Rev. Neurosci. *27*, 549–579.

Ichise, T., Kano, M., Hashimoto, K., Yanagihara, D., Nakao, K., Shigemoto, R., Katsuki, M., and Aiba, A. (2000). mGluR1 in cerebellar Purkinje cells essential for long-term depression, synapse elimination, and motor coordination. Science *288*, 1832–1835.

Kakizawa, S., Yamasaki, M., Watanabe, M., and Kano, M. (2000). Critical period for activity-dependent synapse elimination in developing cerebellum. J. Neurosci. *20*, 4954–4961.

Kano, M., Hashimoto, K., Chen, C., Abeliovich, A., Aiba, A., Kurihara, H., Watanabe, M., Inoue, Y., and Tonegawa, S. (1995). Impaired synapse elimination during cerebellar development in PKCγ mutant mice. Cell *83*, 1223–1231.

Kano, M., Hashimoto, K., Kurihara, H., Watanabe, M., Inoue, Y., Aiba, A., and Tonegawa, S. (1997). Persistent multiple climbing fiber innervation of cerebellar Purkinje cells in mice lacking mGluR1. Neuron *18*, 71–79.

Kano, M., Hashimoto, K., Watanabe, M., Kurihara, H., Offermanns, S., Jiang, H., Wu, Y., Jun, K., Shin, H.S., Inoue, Y., et al. (1998). Phospholipase Cβ4 is specifically involved in climbing fiber synapse elimination in the developing cerebellum. Proc. Natl. Acad. Sci. USA *95*, 15724–15729.

Katz, L.C., and Shatz, C.J. (1996). Synaptic activity and the construction of cortical circuits. Science *274*, 1133–1138.

Kiyohara, Y., Endo, K., Ide, C., and Mizoguchi, A. (2003). A novel morphological technique to investigate a single climbing fibre synaptogenesis with a Purkinje cell in the developing mouse cerebellum: DiI injection into the inferior cerebellar peduncle. J. Electron Microsc. (Tokyo) *52*, 327–335.

Knöpfel, T., Anchisi, D., Alojado, M.E., Tempia, F., and Strata, P. (2000). Elevation of intradendritic sodium concentration mediated by synaptic activation of metabotropic glutamate receptors in cerebellar Purkinje cells. Eur. J. Neurosci. *12*, 2199–2204.

Larramendi, L. (1969). Analysis of synaptogenesis in the cerebellum of the mouse. In Neurobiology of Cerebellar Evolution and Development, R. Llinas, ed. (Chicago: American Medical Association/Education and Research Foundation Institute of Biomedical Research), pp. 803–843.

Lichtman, J.W., and Colman, H. (2000). Synapse elimination and indelible memory. Neuron *25*, 269–278.

Lisman, J.E., Raghavachari, S., and Tsien, R.W. (2007). The sequence of events that underlie quantal transmission at central glutamatergic synapses. Nat. Rev. Neurosci. *8*, 597–609.

Lohof, A.M., Delhaye-Bouchaud, N., and Mariani, J. (1996). Synapse elimination in the central nervous system: functional significance and cellular mechanisms. Rev. Neurosci. *7*, 85–101.

Marin-Padilla, M. (1985). Neurogenesis of the climbing fibers in the human cerebellum: a Golgi study. J. Comp. Neurol. *235*, 82–96.

Mason, C.A., and Gregory, E. (1984). Postnatal maturation of cerebellar mossy and climbing fibers: transient expression of dual features on single axons. J. Neurosci. *4*, 1715–1735.

Mason, C.A., Christakos, S., and Catalano, S.M. (1990). Early climbing fiber interactions with Purkinje cells in the postnatal mouse cerebellum. J. Comp. Neurol. *297*, 77–90.

Miura, E., Fukaya, M., Sato, T., Sugihara, K., Asano, M., Yoshioka, K., and Watanabe, M. (2006). Expression and distribution of JNK/SAPK-associated scaffold protein JSAP1 in developing and adult mouse brain. J. Neurochem. *97*, 1431–1446.

Miyazaki, T., Fukaya, M., Shimizu, H., and Watanabe, M. (2003). Subtype switching of vesicular glutamate transporters at parallel fibre-Purkinje cell synapses in developing mouse cerebellum. Eur. J. Neurosci. *17*, 2563–2572.

Miyazaki, T., Hashimoto, K., Shin, H.S., Kano, M., and Watanabe, M. (2004). P/Q-type Ca^{2+} channel α1A regulates synaptic competition on developing cerebellar Purkinje cells. J. Neurosci. *24*, 1734–1743.

Miyazaki, T., Hashimoto, K., Uda, A., Sakagami, H., Nakamura, Y., Saito, S.Y., Nishi, M., Kume, H., Tohgo, A., Kaneko, I., et al. (2006). Disturbance of cerebellar synaptic maturation in mutant mice lacking BSRPs, a novel brain-specific receptor-like protein family. FEBS Lett. *580*, 4057–4064.

Nakagawa, S., Watanabe, M., Isobe, T., Kondo, H., and Inoue, Y. (1998). Cytological compartmentalization in the staggerer cerebellum, as revealed by calbindin immunohistochemistry for Purkinje cells. J. Comp. Neurol. *395*, 112–120.

Neale, S.A., Garthwaite, J., and Batchelor, A.M. (2001). Metabotropic glutamate receptor subtypes modulating neurotransmission at parallel fibre-Purkinje cell synapses in rat cerebellum. Neuropharmacology *41*, 42–49.

Offermanns, S., Hashimoto, K., Watanabe, M., Sun, W., Kurihara, H., Thompson, R.F., Inoue, Y., Kano, M., and Simon, M.I. (1997). Impaired motor coordination and persistent multiple climbing fiber innervation of cerebellar Purkinje cells in mice lacking Gαq. Proc. Natl. Acad. Sci. USA *94*, 14089–14094.

Palay, S.L., and Chan-Palay, V. (1974). Cerebellar Cortex (New York: Springer-Verlag).

Purves, D., and Lichtman, J.W. (1980). Elimination of synapses in the developing nervous system. Science *210*, 153–157.

Ramón y Cajal, S. (1911). Histologie du Systeme Nerveux de L'homme et des Vertebres, Volume II (Paris: Maloine).

Roth, A., and Häusser, M. (2001). Compartmental models of rat cerebellar Purkinje cells based on simultaneous somatic and dendritic patch-clamp recordings. J. Physiol. *535*, 445–472.

Scelfo, B., Strata, P., and Knöpfel, T. (2003). Sodium imaging of climbing fiber innervation fields in developing mouse Purkinje cells. J. Neurophysiol. *89*, 2555–2563.

Smith, M.A., Ellis-Davies, G.C., and Magee, J.C. (2003). Mechanism of the distance-dependent scaling of Schaffer collateral synapses in rat CA1 pyramidal neurons. J. Physiol. *548*, 245–258.

Sugihara, I. (2005). Microzonal projection and climbing fiber remodeling in single olivocerebellar axons of newborn rats at postnatal days 4-7. J. Comp. Neurol. *487*, 93–106.

Wadiche, J.I., and Jahr, C.E. (2001). Multivesicular release at climbing fiber-Purkinje cell synapses. Neuron *32*, 301–313.

Walsh, M.K., and Lichtman, J.W. (2003). In vivo time-lapse imaging of synaptic takeover associated with naturally occurring synapse elimination. Neuron *37*, 67–73.

Yamasaki, M., Hashimoto, K., and Kano, M. (2006). Miniature synaptic events elicited by presynaptic Ca^{2+} rise are selectively suppressed by cannabinoid receptor activation in cerebellar Purkinje cells. J. Neurosci. *26*, 86–95.